

# Visible and Online Detection of Near-Infrared Optical Vortices via Nonlinear Photonic Crystals

Yuan Liu, Wei Chen,\* Wang Zhang, Chao-Qun Ma, Huai-Xi Chen, Yi-Feng Xiong, Rui Yuan, Jie Tang, Peng Chen, Wei Hu, Fei Xu, and Yan-Qing Lu\*

Near-infrared (NIR) optical vortices (OVs), which carry specific orbital angular momentum, are believed to greatly increase the capacity of conventional optical communication systems. However, due to the equipment limits in invisible wavelengths, NIR OVs detection remains a great difficulty. Here, the up-conversion imaging technology is exploited to circumvent using NIR detectors. A lithium niobate crystal with its quadratic susceptibility modulated by a specially designed Dammann vortex grating is fabricated to realize the frequency conversion—from NIR to the visible region—while converting multiplexed OVs to Gaussian modes in specific multichannels. During the detection process, the most of energies of the detected OVs are preserved, which can be considered as online detection. Additionally, at least 400 nm applicable wavelength range of this method is experimentally demonstrated, as well as up to 25 independent detection channels. Compared with existing solutions, this scheme enables a large-broadband wavelength, low energy loss, and multiprocessing channels platform for visible detection of NIR OVs, showing great potential to be applied in optical communication systems.

## 1. Introduction

Featured by a helical wavefront, a doughnut-like intensity distribution and a central phase singularity, optical vortices (OVs)


Y. Liu, W. Chen, W. Zhang, C.-Q. Ma, Y.-F. Xiong, R. Yuan, P. Chen, W. Hu, F. Xu, Y.-Q. Lu

National Laboratory of Solid State Microstructures  
Key Laboratory of Intelligent Optical Sensing and Manipulation  
College of Engineering and Applied Sciences and Collaborative  
Innovation Center of Advanced Microstructures  
Nanjing University  
Nanjing 210093, China  
E-mail: wchen@nju.edu.cn; yqlu@nju.edu.cn

H.-X. Chen  
Key Laboratory of Optoelectronic Materials Chemistry and Physics  
Fujian Institute of Research on the Structure of Matter  
Chinese Academy of Sciences  
Fuzhou, Fujian 350002, China

H.-X. Chen  
Chinese Academy of Sciences  
University of Chinese Academy of Sciences  
Beijing 100049, China

J. Tang  
Department of Physics  
Nantong University  
Nantong 226019, China

 The ORCID identification number(s) for the author(s) of this article can be found under <https://doi.org/10.1002/adom.202101098>.

DOI: 10.1002/adom.202101098

have been extensively investigated in the past three decades.<sup>[1,2]</sup> Theoretically, OVs carry well-defined orbital angular momentum (OAM),<sup>[1]</sup> which adds a new degree of freedom in beam steering and have been applied in both classical and quantum regions of light.<sup>[3–6]</sup> Compared with the visible beam, the near-infrared (NIR) beam has a series of unique advantages, such as avoiding photo-induced cytotoxicity<sup>[7]</sup> and conveniently generating by traditional lasers.<sup>[8,9]</sup> Especially in the field of optical communication, since the NIR band lies in the low loss and near-zero dispersion area of commercial silica fiber, NIR optical sources have been widely used.<sup>[10,11]</sup> Due to their extra information-carrying capacity, the NIR OVs could profoundly improve the performance of optical communication systems.<sup>[5,12,13]</sup>

The developments of NIR OVs in optical communication generally contain three aspects, transmission, generation, and detection. For transmission, several schemes such as free-space optical transmission,<sup>[5]</sup> spiral fiber,<sup>[12]</sup> and few-mode fiber<sup>[14]</sup> have been demonstrated. Meanwhile, NIR OVs could be generated by spiral phase plates,<sup>[1,15]</sup> *q*-plates,<sup>[16]</sup> fork grating,<sup>[17]</sup> metamaterials,<sup>[18,19]</sup> and so on. Towards detection, most of the methods suggested using various devices, such as linear Dammann gratings,<sup>[20]</sup> spatial light modulator,<sup>[21]</sup> and metasurfaces<sup>[22]</sup> to transform the OVs to Gaussian modes, and then perform detection. However, all these methods cannot be used for online detection due to the transform of the entire incident OVs and the requirement of other devices in the following reconstruction.<sup>[23]</sup> Additionally, despite silicon-based detectors, which have shown excellent quality and high resolution in visible regions, NIR detectors, which are based on InGaAs have been suffered from high readout noise, low-speed response, and stringent cooling requirements.<sup>[23]</sup> Although the above schemes could realize NIR OVs detection, all of them could not avoid using the InGaAs-based detectors, which goes against their applications in optical communications, to a certain extent.

One practical solution is to convert and detect the NIR OVs in visible regions with enhanced imaging performance. Nonlinear up-conversion NIR imaging is conducted in visible regions with high contrast and resolution images captured by silicon charge coupled devices (CCDs).<sup>[24–27]</sup> Earlier research efforts also have proved that, the OAM will be conserved in the nonlinear processes involved with OVs,<sup>[28,29]</sup> which provides a theoretical basis

for visible detection of NIR OV. Besides, nonlinear photonic crystals (NPCs), with asymmetrically modulated quadratic susceptibility, have exhibited a powerful ability of manipulation in nonlinear processes.<sup>[30,31]</sup> Generally, the phase information of the fundamental wave (FW) is preserved when interacted with NPC.<sup>[32]</sup> Still, the change of the FW phase can also happen due to the cascaded spin-orbit angular momentum coupling under special conditions such as illuminating along the optical axis of a BBO crystal with weakly focusing.<sup>[33]</sup> Furthermore, the frequency conversion and the mode transformation of NIR OVs might be realized synchronously by special-designed NPCs.

Here, we propose and demonstrate the visible and online detection of OVs in broadband NIR regions through second harmonic (SH) generation processes in NPCs. An electrically-engineered lithium niobate (LN) crystal with its quadratic nonlinear efficient modulated by a binary Damman vortex gating (DVG) is fabricated to convert the incident NIR OVs. In detail, a genetic algorithm (GA) designed 2D DVG diffracts the OVs to specific orders with equal energies, while others are energy suppressed. In this process, multichannels of NIR OVs could be visibly detected and distinguished due to their transformations to the Gaussian mode. Because of the broadband nature of the three-wave mixing process in NPCs, multiwavelengths of NIR OVs could be detected. Besides, since the linear susceptibility is unmodulated, this method is nondestructive to the incident NIR OVs. Our scheme offers a universal platform for visible and online detection of NIR OVs, which may find applications in optical communication and information processing.

## 2. Principle

2D modulation to the second order nonlinear coefficients of NPCs enables wavefront manipulation of the generated SH beam along the transverse coordinate.<sup>[30,32]</sup> Domain engineered nonlinear crystal with periodically positive and negative quadratic susceptibility induces the  $\pi$  phase difference through the three-wave mixing process. According to the binary-computer generated holograms, a binary phase mask containing phase and amplitude information of light beam enables to support the dynamic optical field manipulation.<sup>[34]</sup> It could be utilized to modulate the sign of nonlinear coefficient as,

$$\chi^{(2)}(x, y) = d_{ij} \sin \left\{ \cos \left[ \frac{2\pi x}{\Lambda} - \Phi(x, y) \right] - \cos [\pi q(x, y)] \right\} \quad (1)$$

where  $d_{ij}$  is the element of  $\chi^{(2)}$  tensor ( $d_{22}$  is mainly involved in this process).  $\Phi(x, y)$  and  $q(x, y)$  are corresponding to the phase and amplitude of the desired beam in the first diffraction order, respectively.  $\Lambda$  is gating period and designed as 170  $\mu\text{m}$  here, while linear grating  $2\pi x/\Lambda$  provides a reciprocal vector contributing the widely used Raman-Nath diffraction method. The transverse phase mismatch is compensated in this process.<sup>[35–37]</sup>

The DVG patterns are designed by GA, which provide specific multichannels of diffracted OAM states. At first, a 1D binarized grating is divided into 20 equal parts, and phase mutations randomly occur in each part. It is worth noting that the mutation is also binarized, corresponding to positive or negative quadratic susceptibility. Meanwhile, Fourier spectrum

analysis is performed on the 1D grating after each mutation. Then we analyze the difference between the calculated Fourier spectrum (after each mutation) and the ideal Fourier spectrum. The difference could be described as,  $\delta = \|S_{\text{cal}} - S_{\text{ideal}}\|_2 / \|S_{\text{ideal}}\|_2$ , where  $S_{\text{cal}}$  is the calculated Fourier spectrum,  $S_{\text{ideal}}$  the ideal Fourier spectrum, and  $\|\cdot\|_2$  represents the L2-norm. The mutation stops only when the calculated difference  $\delta$  meets a specific stop-criterion we set (in our arrangement, the stop-criterion is 10%). Hence, the required 1D Damman grating (DG) is obtained. By adding a spiral phase factor  $e^{im\phi}$  into this DG, a 1D DVG could be formed. Further vertically combining two 1D DVG, a 2D DVG with specific diffraction energy and OAM states distribution could be produced.

Figure 1a shows the binary phase mask to modulate LN domains with different signs. The circular edge design is used to suppress square hole diffraction. A  $2 \times 5$  OAM array could be generated with topological charges of the even numbers for detection (Figure 1b). This scheme is designed to concentrate the converted diffraction energy to the designed orders equally, while other diffraction orders are suppressed. The simulation results in Figure 1b show that the circular-edge design could diffract the unwanted lights (due to the finite size of the phase pattern) as the ring-shape rather than the cross-shape (if using the square-edge design). Thus, the stray lights will not interfere with the diffracted OAM modes. Figure 1c shows the designed diffraction energy distribution.

Here, the liquid crystal (LC)  $q$ -plates are employed to conveniently generate different OAM states through spin-to-orbital angular momentum conversion.<sup>[16]</sup> It has space-variant director distribution depicted by  $\alpha = q\theta + \alpha_0$ , where  $q$ ,  $\theta$  is the topological charge and azimuthal angle, respectively.  $\alpha_0$  is the initial orientation and is assumed to be zero here. Since LC  $q$ -plate is a geometric phase optical element, the generated OV beam carries the topological charge  $2q$ , whose sign is dependent on the incident circular polarization. In addition, the output beam will have a circular polarization converted because the LC  $q$ -plate works as a half-wave plate.

With the generated OV beams illuminating on the LN crystal with second order nonlinear coefficient engineered by DVG, the three-wave mixing process of this process could be described as

$$\begin{aligned} \frac{dA_{2\omega}}{dz} &= \kappa A_{\omega}^2 \cdot \exp[i(2k_1 - k_{2z})z - ik_{2x}x - ik_{2y}y] \cdot \exp(i4q\phi) \\ &\cdot \sum_{n_x=-\infty}^{+\infty} \sum_{n_y=-\infty}^{+\infty} C_n \exp[i2\pi(n_x x/\Lambda_x + n_y y/\Lambda_y)] \\ &\cdot \exp[i(n_x m_x + n_y m_y)\phi] \\ &= \kappa A_{\omega}^2 \sum_{n_x=-\infty}^{+\infty} \sum_{n_y=-\infty}^{+\infty} C_n \exp[i(n_x m_x + n_y m_y + 4q)\phi] \\ &\cdot \exp[i(2k_1 - k_{2z})z] \cdot \exp(i2\pi n_x x/\Lambda_x - ik_{2x}x) \\ &\cdot \exp(i2\pi n_y y/\Lambda_y - ik_{2y}y) \\ &= \kappa A_{\omega}^2 \sum_{n_x=-\infty}^{+\infty} \sum_{n_y=-\infty}^{+\infty} C_n \cdot \exp[i(n_x m_x + n_y m_y + 4q)\phi] \\ &\cdot \exp[i(2k_1 - k_{2z})z] \end{aligned} \quad (2)$$

where  $\kappa$  is the nonlinear coupling coefficient,  $A_{\omega}$ ,  $A_{2\omega}$  the amplitudes of NIR FW and visible SH beam, and  $k_1$ ,  $k_2$  the

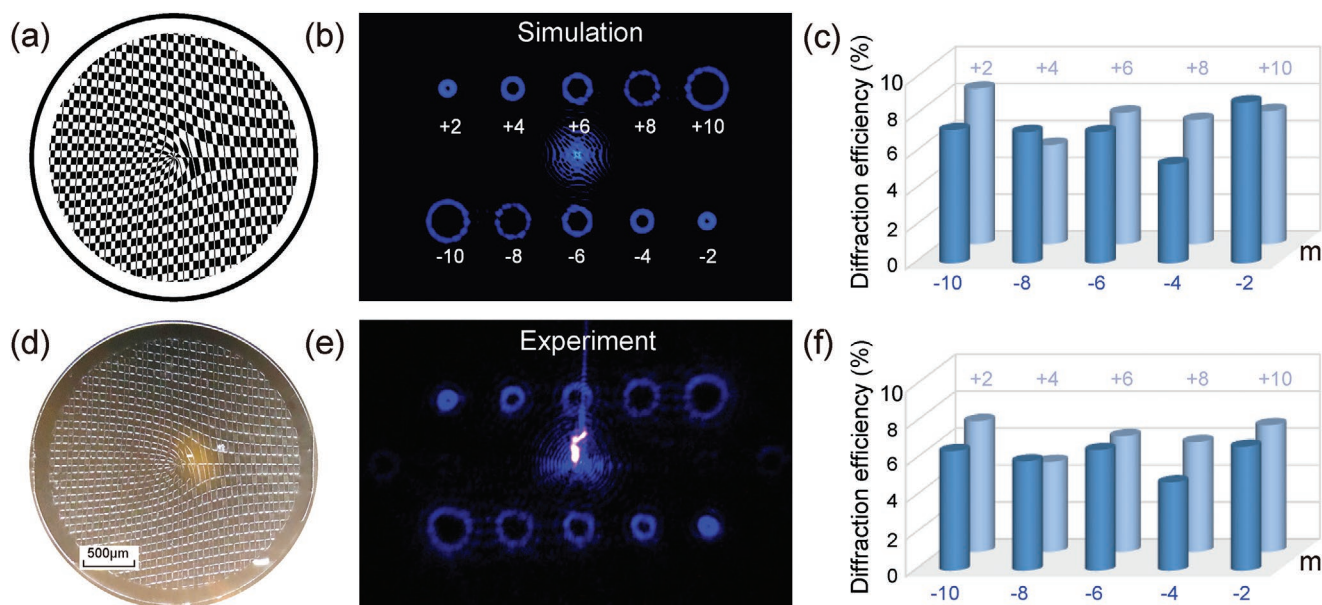


**Figure 1.** a) Designed DVG phase mask with black and white stripes representing 0 and  $\pi$  phase. d) Corresponding sample capture observed by polarization microscope. Scale bar indicates 500  $\mu\text{m}$ . b), e) Simulative and experimental results of diffracted OAM arrays with the topological charge from  $-10$  to  $+10$  and c), f) the corresponding diffraction efficiency of different diffraction orders.

wave-vectors. In Raman–Nath diffraction, the transverse phase matching condition is satisfied, thus the transverse component in Equation (2) is approximating 1, while, the longitudinal direction remains phase-mismatched as expressed by the right term.  $4q\varphi$  in Equation (2) donates the spiral phase factor converted in the SHG process, according to the original OV state generated from the LC  $q$ -plate while considering the fact that the total angular momentums are conserved in this frequency-doubling process. Factor  $C_n$  is the coefficient of  $n$ th diffraction order, which is connected to equal distribution diffraction power normalized with respect to the total power. Different orders carry topological charges of  $n_x m_x + n_y m_y + 4q$ . Under the condition of  $n_x m_x + n_y m_y + 4q = 0$ , the corresponding OVs (generated from geometrical phase LC  $q$ -plate) are converted to Gaussian mode with a bright spot in the center of the specific diffraction orders. Since the generated SH beam is in the visible regions, these diffraction patterns could be directly captured by CCD wherein the filled dots will be easily distinguished.

### 3. Results

In order to encode the designed DVG phase mask to the quadratic susceptibility of LN nonlinear crystal, the electric poling method is adopted in the sample preparation process.<sup>[38,39]</sup> The  $+z$  face of a  $z$ -cut LN slice is covered with a 120-nm-thick Cr electrode having the designed DVG pattern, through the process of maskless photolithography, vacuum deposition, and photoresist removal. High voltage pulses slightly larger than the coercive field of the used 50- $\mu\text{m}$ -thick LN slice are applied to convert the spontaneous polarization directions. LN domains with the designed DVG space-variant patterns could be observed by a polarization optical microscope because of the existence of slight stress in the domain walls (Figure 1d).

The FW beam experiences a  $\pi$ -phase difference when propagates along the  $z$ -axis due to the changing signs of  $d_{22}$  in the fabricated NPC. Multichannels of designed spatially distributed OAM states ( $-10$  to  $+10$ ) in  $2 \times 5$  diffraction orders are experimentally generated in Figure 1e. The generated OAM arrays have an expected diffraction efficiency with approximately equal energy distribution, which is consistent with the theoretical prediction (Figures 1c–f). The geometric phase element LC  $q$ -plates is fabricated through photoalignment technology carried out by a digital-micromirror-device based microlithography setup.<sup>[40]</sup> The illustration in Figure 2a indicates the theoretical director and phase distribution of LC  $q$ -plate ( $q = 0.5$ ). Figure 2b,e,h,k is the image of LC  $q$ -plate with  $q = 0.5$  and  $q = 1$  under polarization optical microscope, whose color variation reveals the continuous change of LC director from  $0^\circ$  to  $180^\circ$ .

NIR OVs generated from LC  $q$ -plate with different spins and orbital angular momentums could be visibly detected simultaneously through the nonlinear diffraction process deduced by LN DVG domain structure. Figure 2a shows the experimental set-up. A Ti:sapphire femtosecond laser (Revolution, Coherent, USA) pumped optical parametrical amplifier (TOPAS-Prime, Light Conversion, Lithuania) is utilized as the light source with a pulse duration of 50 fs and a repetition rate of 1 kHz. A linearly polarized NIR 900 nm laser beam is firstly adopted with its energy adjusted by an attenuation pad. A 4f optical system combined with two spherical lenses ( $f = 500$  and 200 mm) expands and collimates the incident beam to match the size of the LN phase mask. By rotating the first QWP with an angle of  $45^\circ$  to the original polarization direction, the right circular polarized incident beam directly illuminates onto LC  $q$ -plate with  $q = 0.5$ . Generated OV ( $m = -1$ ) in Figure 2c could be detected in Figure 2d since the original OAM channel ( $m = +2$ ) in the left corner is converted to Gaussian mode according to Equation (2). Meanwhile, due to spin-to-orbital



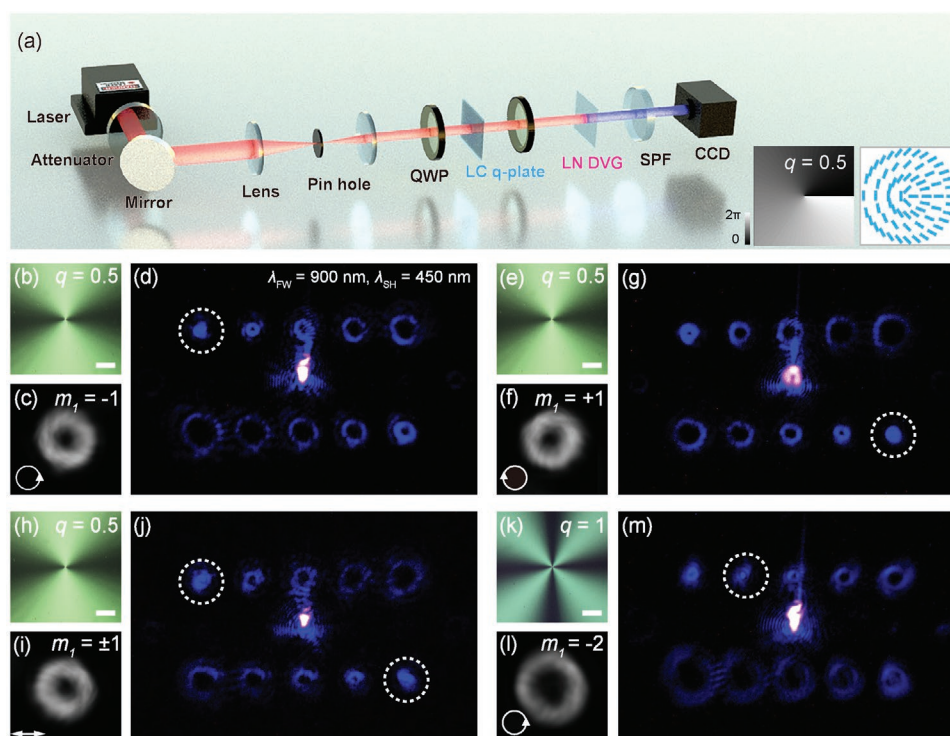


**Figure 2.** a) Experimental set-up for multichannel OAM detection in NIR regions. QWP, quarter-wave plate. SPF, short pass filter. Inserted pictures are theoretical phase patterns and LC director distribution. b), e), h), k) Images of LC  $q$ -plate with  $q = 0.5$  and  $q = 1$  under crossed polarizations. Scale bar indicates  $500 \mu\text{m}$ . c), f), i), l) Generated OVs with incident left, right circular, and linear polarizations, respectively. d), g), j), m) Corresponding detection results: diffraction patterns with NIR  $900 \text{ nm}$  FW incident beam converted to visible  $450 \text{ nm}$  SH beam. Filled dots circled by a dashed line indicates the detected OVs mode.

angular momentum conversion of LC  $q$ -plate, by rotating the QWP angle to  $-45^\circ$ , a topological charge of  $m = +1$  (Figure 2f) with opposite circular polarization could be detected in the bottom row, as shown in Figure 2g. Furthermore, by illuminating the LC  $q$ -plate with a linearly polarized incident beam, the generated beam can be considered as the superimposing of a left-circularly polarized beam with the topological charge of  $m = -1$  and a right-circularly polarized beam with the topological charge of  $m = +1$  (Figure 2i).<sup>[41]</sup> Our results in Figure 2j show that mixed topological charges ( $m = \pm 1$ ) could be simultaneously detected in two independent channels, which confirms the ability of this method for demultiplexing of coherent superposition of optical vortices. Limited by current research conditions, the ability of this method of demultiplexing for mixed OVs under incoherent superposition (which can also be encountered in telecommunication applications) may require further investigation. OV beam carrying OAM ( $m = -2$ ) generated by  $q$ -plate with  $q = 1$  converts the second point to Gaussian mode in the upper row of OAM array, as presented in Figure 2k, m, l. LN DVG is employed as a nonlinear beam convertor and diffraction OAM array generator. In addition, the SH beam ( $450 \text{ nm}$ ) is filtered out by SPF, then the detection patterns with visible blue color could be directly captured by a CCD. Besides, due to the ultrafast response of the nonlinear conversion process (which has been recently demonstrated to allow spatially distinguishing the temporal evolution of spectral components), this technique has the potential to be used in OAM demultiplexing in the time domain.<sup>[27]</sup>

Meanwhile, broadband NIR region OAM states could be conveniently detected due to the excellent wavelength tolerance in the nonlinear diffraction of LN DVG through a three-wave mixing process. By switching the output wavelengths of the OPA module, the FW OV beams of  $1150$  and  $1300 \text{ nm}$  are obtained experimentally. In the SH generation process, it could be converted with doubled topological charges and detected by diffraction orders of OAM states in visible wavelengths of  $575 \text{ nm}$  (Figure 3a) and  $650 \text{ nm}$  (Figure 3b), respectively. Since the original  $m = +2$  OAM order is reduced to Gaussian mode, a left circular polarized OV with a topological charge of  $m = -1$  could be assumed. The wavelength compatibility of the nonlinear process results in a larger wavelength detection range, which is difficult to be realized with traditional liquid crystal devices or metamaterials. Furthermore, by redesigning the phase mask of DVG, larger dynamic OAM arrays ( $5 \times 5$ ) with more NIR detection channels could be obtained (Figure 3c). Detection results of OV generated from LC  $q$ -plate with  $q = 0.5$  with left circular polarization are shown in Figure 3d.

The non-perturbing feature and low energy loss property of this method are experimentally demonstrated. Since quadratic NPCs are electrically poled with only the second order susceptibility spatially modulated, while the linear susceptibility remains constant,<sup>[32]</sup> the FW of OVs could pass through directly without mode damage.<sup>[42]</sup> Figure 4a is the capture of under-detected OV with the topological charge of  $m = +2$  after passing through the detection sample NPC, which remains the typical donut shape of OVs. The inserted capture in the left corner is the original

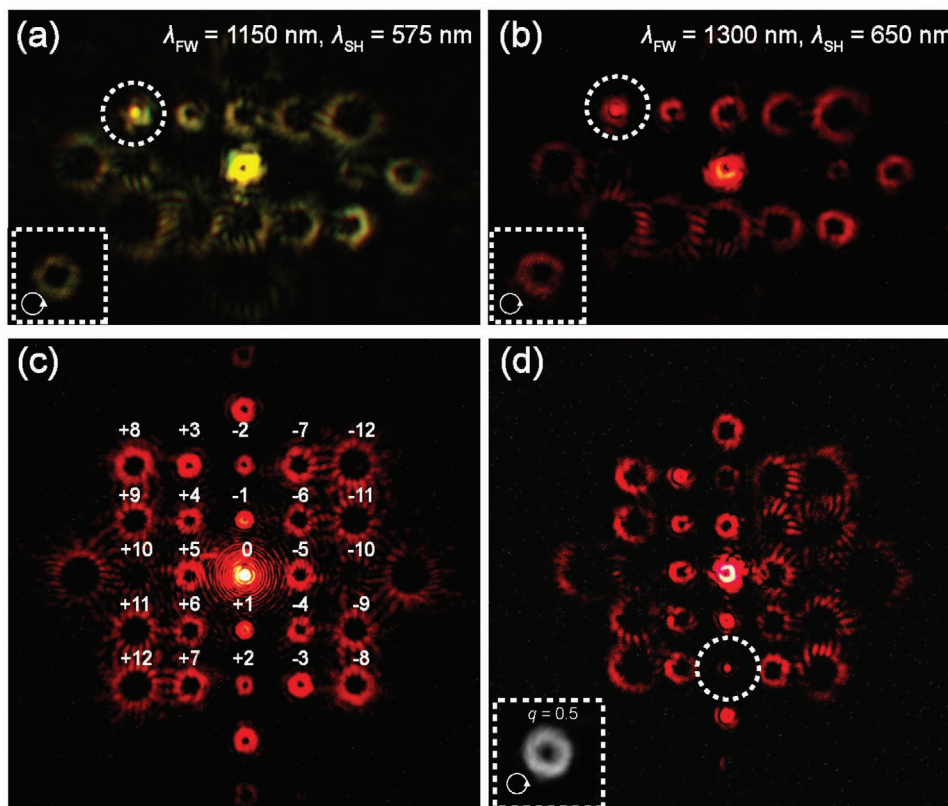


**Figure 3.** a,b) Broadband OAM state (e.g.,  $m = -1$ ) detection results with wider incident NIR wavelength ( $\lambda_{FW} = 1150$  nm and  $\lambda_{FW} = 1300$  nm) and corresponding visible SH diffraction patterns (yellow and red). c) A 5×5 nonlinear diffracted OAM array with topological charges from -12 to +12. d) Detected capture of OV outputs from LC  $q$ -plate ( $q = 0.5$ ) with incident beam in right circular polarization. Filled dots circled by a dashed line indicate the converted Gaussian mode.

FW beam before the NPC sample. These two beams are almost the same, except for a slight intensity difference. Figure 4b is generated SH OV with the topological charge of  $m = +4$  near the NPC surface. The domain structures of the NPC sample could also be distinguished in the captured background. The input OAM states are detected without disturbing the original mode and wavefront. Furthermore, to exact the energy loss level of this method, the nonlinear conversion efficiency is measured in the experiment. Figure 4c shows that the converted SH beam power has a quadratic function dependence on the pump beam, being consistent with the theoretical prediction.<sup>[43]</sup> While the SH generation efficiency has a linear relationship of the fundamental beam power (Figure 4d), since the nonlinear efficiency is defined as  $\eta = \langle P_{2\omega} \rangle / \langle P_{\omega} \rangle$ , where  $\langle P_{2\omega} \rangle$  is the average SH beam power and  $\langle P_{\omega} \rangle$  is the average FW beam power. Thus, the nonlinear conversion efficiency is about the order of  $10^{-5}$ , which indicates a quite low loss of the energy of the FW beam. Visible detection of NIR OAM by NPC can be considered as a nondestructive method and has the potential to be applied in more laser beam detection and conversion process.

#### 4. Discussion and Conclusion

The current approach does not exhaust all the possibilities. We note that using 1D nonlinear DVG to generate OVs with

controllable diffraction energies has been investigated.<sup>[44]</sup> Nevertheless, our results show the possibility of further generating large-scale 2D OAM arrays (Figure 3c). Building a NIR laser with such NPCs in the cavity will realize an OVs source that works in the visible region. Besides, in some practical applications (especially when the energies of NIR OVs are quite weak), it is necessary to improve the nonlinear conversion efficiency to achieve effective detection. By further adopting the 3D NPCs which have been demonstrated in recent years, the nonlinear conversion efficiency of this method could be tailored even being comparable to the typical quasi phasing-matching condition, which allows us to make a trade-off between improving conversion efficiency and reducing signal loss in practical applications.<sup>[45]</sup> Furthermore, new advanced materials especially those that have broadband properties, such as multiple-twist, single-pitch, or gradient helical liquid crystal strategy, have the potential to be combined with such NPCs.<sup>[46–49]</sup> Due to the enhanced polarization-dependent response, this combination might enable more functionalities such as the detection of spin angular momentum and dynamic generation of other structured lights, which could broaden the practical application environments of this method.

In conclusion, a visible and online detection scheme for NIR OVs is demonstrated through the nonlinear diffraction process in an electrically-poled LN slice, whose quadratic susceptibility is modulated by a specifically designed DVG. This

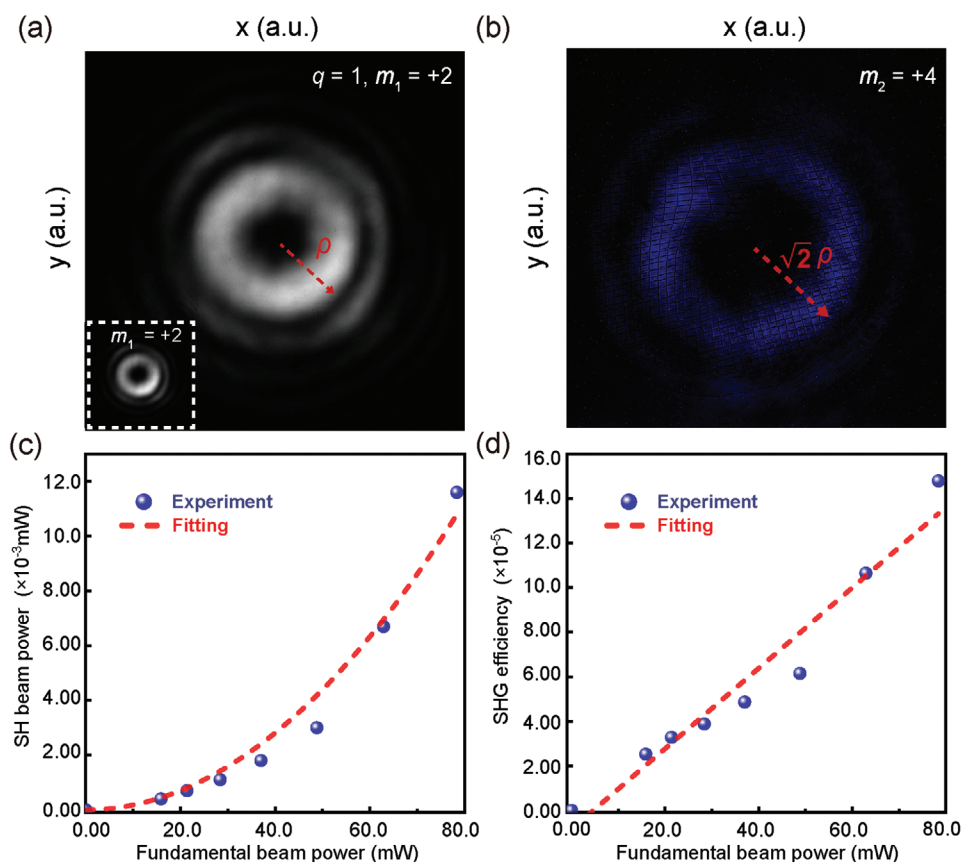


**Figure 4.** a) Beam pattern capture of the under-detected OV with the topological charge of  $m = +2$  after passing through the detection sample NPC, and the inserted capture in the left corner is the original FW beam before NPC. b) Beam pattern capture of generated SH OV with the topological charge of  $m = +4$  near the NPC surface. The red arrow indicates the radius of the corresponding OVs. c,d) SH beam power and nonlinear conversion efficiency as a function of the pump input beam power. SHG, second harmonic generation.

arrangement has three main advantages: (1) The frequency conversion and the mode transformation are performed simultaneously, which greatly reduces the complexity of the system; (2) It could be applied to a large-broadband wavelength; (3) It is nondestructive to the fundamental NIR OVs and could be used for online detection. More specifically,  $2 \times 5$  or  $5 \times 5$  diffraction detection channels of OVs carrying topological charges from  $-5$  to  $+5$  ( $-6$  to  $+6$ ) with circular and linear polarization are experimentally demonstrated. It is demonstrated that NIR OVs with wavelengths from 900 to 1300 nm could be converted to the corresponding visible OVs and then directly captured by the silicon-based CCD camera. Low energy loss and slight mode damage to the FW beam are also confirmed in the experiment. We believe that this method is well-suited for NIR OVs detection and optical information processing in optical communication.

## Acknowledgements

Y.L., W.C., and W.Z. contributed equally to this work. This work was supported by the National Key Research and Development Program of China (2017YFA0303700), the National Natural Science Foundation of China (NSFC) (12004200, 12004175), the Natural Science Foundation of Jiangsu Province (No. BK20200311).

## Conflict of Interest

The authors declare no conflict of interest.

## Data Availability Statement

Research data are not shared.

## Keywords

near-infrared detection, nonlinear photonic crystals, optical vortex

Received: June 1, 2021  
Revised: September 8, 2021  
Published online: October 11, 2021

- [1] L. Allen, M. W. Beijersbergen, R. J. C. Spreeuw, J. P. Woerdman, *Phys. Rev. A* **1992**, 45, 8185.
- [2] Y. Shen, X. Wang, Z. Xie, C. Min, X. Fu, Q. Liu, M. Gong, X. Yuan, *Light: Sci. Appl.* **2019**, 8, 90.
- [3] D. G. Grier, *Nature* **2003**, 424, 810.
- [4] M. Padgett, R. Bowman, *Nat. Photonics* **2011**, 5, 343.



- [5] J. Wang, J. Y. Yang, I. M. Fazal, N. Ahmed, Y. Yan, H. Huang, Y. Ren, Y. Yue, S. Dolinar, M. Tur, A. E. Willner, *Nat. Photonics* **2012**, *6*, 488.
- [6] A. Mair, A. Vaziri, G. Weihs, A. Zeilinger, *Nature* **2001**, *412*, 313.
- [7] Y. Yang, J. Aw, B. Xing, *Nanoscale* **2017**, *9*, 3698.
- [8] D. J. Richardson, J. Nilsson, W. A. Clarkson, *J. Opt. Soc. Am. B* **2010**, *27*, B63.
- [9] I. D. W. Samuel, G. A. Turnbull, *Chem. Rev.* **2007**, *107*, 1272.
- [10] E. Agrell, M. Karlsson, A. R. Chraplyvy, D. J. Richardson, P. M. Krummrich, P. Winzer, K. Roberts, J. K. Fischer, S. J. Savory, B. J. Eggleton, M. Secondini, F. R. Kschischang, A. Lord, J. Prat, I. Tomkos, J. E. Bowers, S. Srinivasan, M. Brandt-Pearce, N. Gisin, *J. Opt.* **2016**, *18*, 063002.
- [11] H. Ren, X. Li, Q. Zhang, M. Gu, *Science* **2016**, *352*, 805.
- [12] N. Bozinovic, Y. Yue, Y. Ren, M. Tur, P. Kristensen, H. Huang, A. E. Willner, S. Ramachandran, *Science* **2013**, *340*, 1545.
- [13] X. Fang, H. Yang, W. Yao, T. Wang, Y. Zhang, M. Gu, M. Xiao, *Adv. Photon.* **2021**, *3*, 015001.
- [14] B. Ndagano, R. Bruning, M. McLaren, M. Duparre, A. Forbes, *Opt. Express* **2015**, *23*, 17330.
- [15] E. Stegemburgs, A. Bertoni, A. Trichili, M. S. Alias, T. K. Ng, M. S. Alouini, C. Liberale, B. S. Ooi, *IEEE Commun. Mag.* **2019**, *57*, 65.
- [16] L. Marrucci, C. Manzo, D. Paparo, *Phys. Rev. Lett.* **2006**, *96*, 163905.
- [17] B. Y. Wei, W. Hu, Y. Ming, F. Xu, S. Rubin, J. G. Wang, V. Chigrinov, Y. Q. Lu, *Adv. Mater.* **2014**, *26*, 1590.
- [18] Y. Bao, J. Ni, C. W. Qiu, *Adv. Mater.* **2019**, *32*, 1905659.
- [19] N. Yu, P. Genevet, M. A. Kats, F. Aieta, J. P. Tetienne, F. Capasso, Z. Gaburro, *Science* **2011**, *334*, 333.
- [20] N. Zhang, X. C. Yuan, R. E. Burge, *Opt. Lett.* **2010**, *35*, 3495.
- [21] J. Pinnell, V. Rodríguez Fajardo, A. Forbes, *Opt. Express* **2019**, *27*, 28009.
- [22] S. Zhang, P. Huo, W. Zhu, C. Zhang, P. Chen, M. Liu, L. Chen, H. J. Lezec, A. Agrawal, Y. Lu, T. Xu, *Laser Photonics Rev.* **2020**, *14*, 2000062.
- [23] A. Rogalski, *Infrared Phys. Technol.* **2002**, *43*, 187.
- [24] J. E. Midwinter, *Appl. Phys. Lett.* **1968**, *12*, 68.
- [25] A. H. Firester, *J. Appl. Phys.* **1970**, *41*, 703.
- [26] X. Qiu, F. Li, W. Zhang, Z. Zhu, L. Chen, *Optica* **2018**, *5*, 208.
- [27] M. Mrejen, Y. Erlich, A. Levanon, H. Suchowski, *Laser Photonics Rev.* **2020**, *14*, 2000040.
- [28] K. Dholakia, N. B. Simpson, M. J. Padgett, L. Allen, *Phys. Rev. A* **1996**, *54*, R3742.
- [29] G. H. Shao, Z. J. Wu, J. H. Chen, F. Xu, Y. Q. Lu, *Phys. Rev. A* **2013**, *88*, 063827.
- [30] T. Ellenbogen, N. Voloch-Bloch, A. Ganany-Padowicz, A. Arie, *Nat. Photonics* **2009**, *3*, 395.
- [31] N. V. Bloch, K. Shemer, A. Shapira, R. Shiloh, I. Juwiler, A. Arie, *Phys. Rev. Lett.* **2012**, *108*, 233902.
- [32] A. Arie, N. Voloch, *Laser Photonics Rev.* **2010**, *4*, 355.
- [33] Y. Tang, K. Li, X. Zhang, J. Deng, G. Li, E. Brasselet, *Nat. Photonics* **2020**, *14*, 658.
- [34] W. H. Lee, *Appl. Opt.* **1979**, *18*, 3661.
- [35] A. Shapira, R. Shiloh, I. Juwiler, A. Arie, *Opt. Lett.* **2012**, *37*, 2136.
- [36] S. M. Saltiel, D. N. Neshev, W. Krolikowski, A. Arie, O. Bang, Y. S. Kivshar, *Opt. Lett.* **2009**, *34*, 848.
- [37] X. Hu, Y. Zhang, S. Zhu, *Adv. Mater.* **2020**, *32*, 1903775.
- [38] M. Y. Wang, J. Tang, H. J. Wang, Y. Ming, Y. Zhang, G. X. Cui, Y. Q. Lu, *Appl. Phys. Lett.* **2018**, *113*, 081105.
- [39] Y. Liu, W. Chen, J. Tang, X. Xu, P. Chen, C. Q. Ma, W. Zhang, B. Y. Wei, Y. Ming, G. X. Cui, Y. Zhang, W. Hu, Y. Q. Lu, *Adv. Opt. Mater.* **2021**, *9*, 2001776.
- [40] P. Chen, B. Y. Wei, W. Hu, Y. Q. Lu, *Adv. Mater.* **2020**, *32*, 1903665.
- [41] G. Milione, H. I. Sztul, D. A. Nolan, R. R. Alfano, *Phys. Rev. Lett.* **2011**, *107*, 053601.
- [42] D. Wei, Y. Zhu, W. Zhong, G. Cui, H. Wang, Y. He, Y. Zhang, Y. Lu, M. Xiao, *Appl. Phys. Lett.* **2017**, *110*, 261104.
- [43] R. W. Boyd, *Nonlinear Optics*, Elsevier and Academic Press, London, UK **2008**.
- [44] H. Wang, D. Wei, X. Xu, M. Wang, G. Cui, Y. Lu, Y. Zhang, M. Xiao, *Appl. Phys. Lett.* **2018**, *113*, 221101.
- [45] D. Wei, C. Wang, H. Wang, X. Hu, D. Wei, X. Fang, Y. Zhang, D. Wu, Y. Hue, J. Lie, S. Zhu, M. Xiao, *Nat. Photonics* **2018**, *12*, 596.
- [46] Y. Li, J. Kim, M. J. Escuti, *Proc. SPIE* **2012**, *8274*, 827415.
- [47] M. Rafayelyan, E. Brasselet, *Opt. Lett.* **2016**, *41*, 3972.
- [48] J. Kobashi, H. Yoshida, M. Ozaki, *Phys. Rev. Lett.* **2016**, *116*, 253903.
- [49] M. Rafayelyan, G. Agez, E. Brasselet, *Phys. Rev. A* **2017**, *96*, 043862.